Journal of Catalysis **186,** 110–122 (1999)
Article ID jcat.1999.2536, available online at http://www.idealibrary.com on IDEAL®

Preparation, Characterization, and Catalytic Activity of Molybdenum Carbide or Nitride Supported on Platinum Clusters Dispersed in EMT Zeolite

Thierry Bécue, Jean-Marie Manoli, Claude Potvin, Robert J. Davis,* and Gérald Djéga-Mariadassou[1]

*Laboratoire Réactivité de Surface, Université P. & M. Curie, CNRS-UMR 7609, 4 Place Jussieu, Casier 178, 75252 Paris Cedex 05, France; and *Department of Chemical Engineering, University of Virginia, Charlottesville, Virginia 22903*

Received January 8, 1999; revised April 15, 1999; accepted April 20, 1999

Bimetallic Pt–Mo catalysts were prepared by vapor deposition of $Mo(CO)_6$ onto nanometer size platinum particles previously dispersed on EMT zeolite. Subsequent decomposition of the Mo precursor formed a supported molybdenum carbide phase whereas reaction of the precursor with ammonia formed a supported nitride phase. Results from high-resolution transmission electron microscopy and X-ray absorption spectroscopy at the Mo K and Pt LIII edges showed conclusively that highly dispersed particles containing both transition metals were synthesized by the vapor deposition method. Coverage of Pt by Mo suppressed both the total capacity for dihydrogen chemisorption and the catalytic activity for benzene hydrogenation. However, compared to monometallic Mo carbide or nitride clusters supported on EMT zeolite, the bimetallic catalysts were much more active in the catalytic reactions of *n*-heptane at 623 K. The low thickness of the carbide or nitride phase (about 0.3 nm) allowed for a synergistic influence of the Mo phase on the small areas of exposed Pt and/or a direct activation of the nitride or carbide for catalysis.

1. INTRODUCTION

High surface area transition metal carbides and nitrides present promising catalytic activities in several processes (1, 2). Since these reactions are typically catalyzed by noble metals, the potential for using carbides and nitrides instead of noble metals motivates intensive research on the synthesis and catalytic function of these compounds. Usually, catalysis by carbides and nitrides is found to be strongly related to their surface structure and elemental composition, which depend on their synthesis procedure. Transition metal carbides or nitrides are typically obtained by a temperature-programmed reaction of an oxide precursor with a CH_4/H_2 mixture or NH_3 (3–5). Since heterogeneous catalytic reactions require the reactants to interact with active sites located exclusively on the surface, conversion of the whole transition metal oxide precursor into a carbide or nitride may not be necessary (6). Indeed, a surface carbide or nitride layer supported on a bulk-phase oxide may exhibit a different catalytic activity compared to that of a bulk-phase carbide or nitride, and such a phenomenon can be related to the well-known concept of metal–support interaction in catalysis by metals. A goal of this study was to perform catalytic investigations on bimetallic carbide (Pt–MoC) and nitride (Pt–MoN) catalysts to determine if a synergism exists between carbide or nitride monolayers and their underlying platinum core. According to the procedure of Tri *et al.* (7), Mo layers were selectively deposited from nonoxidic precursors onto Pt nanoclusters supported on EMT zeolite, a system previously studied in this laboratory (8). Subsequent conversion of the Mo layers into carbides or nitrides completed the preparation of highly dispersed bimetallic clusters. The catalytic activities and selectivities of these compounds in the transformations of *n*-heptane have been compared to those of bulk Mo_2C and Mo_2N as well as zeolite-supported molybdenum carbide or nitride.

2. EXPERIMENTAL METHODS

2-1. Preparation of Catalysts

The EMT zeolite (Si/Al = 3.8, $S_{BET} = 670$ m^2 g^{-1}) was synthesized in a pure form using a slightly modified procedure based on that of Delprato *et al.* (9). Zeolite-supported Pt–Mo bimetallic clusters were prepared by first supporting platinum clusters on the sodium form of zeolite EMT (designated as Pt3/NaEMT and Pt6/NaEMT for 3 and 6% Pt by weight, respectively) according to the ion-exchange method of Dalla Betta and Boudart (10) and by treating the samples as described previously (8).

A quartz reactor containing the platinum clusters supported on zeolite was connected, via a grease-free stopcock and without exposure to air, to a cell containing the required amount of degassed $Mo(CO)_6$. This method used by Tri *et al.* (7) allowed us to control the amount of molybdenum loaded onto the sample. The vapor deposition was carried out at room temperature for about 2 days and was followed

[1] To whom correspondence should be addressed. Fax: (33) 1 44276033. E-mail: jmm@ccr.jussieu.fr.

0021-9517/99 $30.00

either by a decomposition at 600 K (heating rate, 1 K min^{-1}) in a partial pressure of H_2 (4×10^4 Pa [300 Torr]) and an evacuation at 600 K to remove the carbonyl ligands or by a nitridation at 973 K in flowing ammonia (6 L h^{-1}). Tri *et al.* observed that the Mo distribution was inhomogeneous for samples having an atomic ratio Pt/(Pt + Mo) smaller than 0.5. Thus, to obtain a Mo/Pt atomic ratio greater than unity and to ensure that $Mo(CO)_6$ can access the zeolite cages and cover the platinum particles, successive exposures of a sample to $Mo(CO)_6$ were carried out with each step having a Mo/Pt atomic ratio less than 1. Between each stage, the molybdenum hexacarbonyl was thermally decomposed at 600 K under a partial pressure of H_2 to liberate the zeolite pores for subsequent deposition of $Mo(CO)_6$. The last vapor deposition was followed by a decomposition of the carbonyl complex in flowing dihydrogen to form the supported carbide or by a nitridation step to form the supported nitride.

For use as reference materials, monometallic molybdenum carbide (MoC/NaEMT) or molybdenum nitride clusters (MoN/NaEMT) on NaEMT (5 wt% Mo) were also prepared by vapor deposition of $Mo(CO)_6$ onto the dehydrated zeolite, followed by a decomposition or a nitridation step, respectively. This procedure is described in detail elsewhere (11). A bulk δ-MoN reference material was prepared by heating (60 K h^{-1}) 1 g of $MoCl_3$ (not exposed to air) under flowing ammonia (10 L h^{-1}) up to 973 K (11). Synthesis of bulk Mo_2N is also described in Ref. (11).

2-2. *Characterization of Catalysts*

The elemental analysis of the solids was obtained from the Service Central d'Analyse du Centre National de la Recherche Scientifique (Vernaison, France).

A Siemens D500 automatic diffractometer with a Cu K_α monochromatized radiation source was used to obtain the X-ray diffraction (XRD) patterns of the various solid phases. The degree of crystallinity of the loaded zeolites was estimated from the intensity of all reflections in the range $2\theta = 14.5-29.3^\circ$ (12) and compared with those of the calcined NaEMT zeolite. For catalysts containing Pt and/or Mo, the measured intensities were corrected for the absorption of X-rays by the heavy atoms (13).

The ^{28}Si and ^{27}Al solid state MAS NMR (magic angle spinning nuclear magnetic resonance) spectra of the hydrated samples were recorded on a Bruker MSL 400 spectrometer (9.4 T) operating at 79.5 MHz and on a Bruker MSL 300 (7.1 T) functioning at 78.2 MHz, respectively.

High-resolution transmission electron microscopy of the catalysts was performed on a Jeol JEM 100 CXII apparatus, equipped with a top entry device and operated at 100 kV. Ultramicrotome sections (80–100 nm) of the samples were prepared for the studies. The EDS results (STEM mode) were obtained using a LINK AN 10000 system connected to a silicon–lithium diode detector and a multichannel analyzer. The EDS analyses were performed on several small domains of the samples (fixed STEM beam analysis areas between 180 and 3000 nm^2).

The X-ray absorption spectra were recorded at the Mo K edge (20000 eV) or the Pt LIII edge (11564 eV) on beam line X10C at the National Synchrotron Light Source, Brookhaven National Laboratory (Upton, NY) in the transmission mode of data collection. The storage ring operated with an electron energy of 2.5 GeV and currents typically ranged from 100 to 300 mA. The intensities of the X-rays exiting the Si(220) double-crystal monochromator and passing through the sample were measured by gas-filled ionization chambers. Harmonic rejection was accomplished by the focusing mirror on the beamline. Each sample was loaded into an *in situ* cell and heated to 673 K in dihydrogen for 30 min and cooled to ambient temperature for collection of spectra. A Pt or Mo metal foil was placed in series with the sample to provide independent calibration of the edge energy. The EXAFS data were processed with Macintosh versions of the University of Washington analysis programs. Structural parameters calculated for supported Pt clusters were referenced to a standard EXAFS function associated with a 4-μm Pt foil recorded at ambient conditions on beam line X18B.

Dihydrogen chemisorption measurements were carried out at 313 K in a conventional high vacuum system equipped with a Datametrics capacitance gauge (type 1014A). The samples were reduced *in situ* in flowing dihydrogen (6 L h^{-1}) by heating at 1 K min^{-1} to 573 K and remaining at 573 K overnight. The reduced samples were then outgassed for 1 h at 673 K to a final pressure of 10^{-4} to 10^{-5} Torr (1 Torr = 133.3 N m^{-2}). The "back-sorption" method of Yates and Sinfelt was used for titration of metallic sites (14). According to this method, evacuation of the sample at the temperature of chemisorption eliminates the physisorbed hydrogen (reversible hydrogen) without displacing chemisorbed hydrogen (irreversible hydrogen). Thus, chemisorption measurements were done by successively increasing the dihydrogen partial pressure over the catalyst bed until saturation of the metallic surface had been obtained. The total number of hydrogen atoms adsorbed (H_{total}) was determined at this stage. Then, the reactor was evacuated (final $P < 5 \times 10^{-5}$ Torr) and another series of chemisorption measurements was used to determine the amount of reversibly adsorbed hydrogen ($H_{reversible}$). The amount of irreversibly adsorbed hydrogen ($H_{irreversible}$) was calculated from

$$H_{irreversible} = H_{total} - H_{reversible}.$$

The percentage of metal exposed was calculated assuming a stoichiometric adsorption of hydrogen atoms on surface platinum atoms (H/Pt ratio equal to 1) (15).

The fraction of platinum atoms exposed (FE Pt) was also estimated by benzene hydrogenation measurements

carried out at 298 K and 760 Torr total pressure in a conventional differential dynamic reactor operating with a total flow rate of 3.6 L min^{-1}. The partial pressure of benzene was chosen to be 58 Torr (molar ratio $H_2/C_6H_6 = 12$) to ensure the reaction was zero order in benzene. Benzene hydrogenation is a structure-insensitive reaction that, by definition, has a turnover rate (rate per second per catalytic site, s^{-1}) that is independent of the exposed crystallographic plane or the catalyst particle size (16, 17). If all exposed metallic atoms are active sites for the reaction, their number density can easily be deduced from the specific rate (rate per second per gram of catalyst) and the known turnover rate at the temperature of the reaction. The turnover rate for benzene hydrogenation on supported Pt at 298 K was measured to be 5.4×10^{-2} and 5.2×10^{-2} s^{-1} for Pt3/NaEMT and Pt6/NaEMT, respectively.

2-3. Reaction of n-Heptane

The *n*-heptane reaction was carried out over 70 mg of catalyst in a flow reactor at 623 K and a total pressure of 760 Torr. The reactor feed was a mixture of dihydrogen and *n*-heptane in a molar ratio of 17 to 1, flowing at 0.012 L min^{-1}. For both benzene hydrogenation and *n*-heptane transformations, the samples were first pretreated at 773 K under flowing dihydrogen for 5 h and cooled to 623 K. The products of reaction were separated and identified by an on-line gas chromatograph (H. P. Model 5890 series II), equipped with a 50-m PLOT capillary column coated with alumina deactivated by KCl, using temperature programming and a FID detector.

3. RESULTS AND DISCUSSION

3-1. Characterization of the Monometallic Platinum Catalysts

We have previously shown (8) that highly dispersed platinum clusters in EMT zeolite can be prepared and that the size of the Pt particles did not depend on the Pt loading. The X-ray diffractograms for the platinum catalysts labeled as Pt*x*/NaEMT (*x* being the Pt loading in weight %) showed good crystallinity of the support. Furthermore, no X-ray diffraction peaks corresponding to the platinum phase were detected. Table 1 summarizes some of the physicochemical characteristics of the supported Pt catalysts. Earlier work proved that the fraction of the platinum atoms exposed in those samples was equal to 1 (8). Additional characterization confirmed that the platinum was dispersed homogeneously throughout the EMT porosity (low standard deviation on several EDS measurements) and that the crystallinity of the samples was preserved in comparison to that of NaEMT. The Si/Al ratio was not altered by catalyst treatment and no ^{28}Si peak corresponding to an amorphous phase was detected at −110 ppm. The ^{27}Al MAS NMR spectra of the different materials presented resonances near 60 ppm specific to tetrahedral aluminium species. After thermal treatments the spectra also contain very weak resonances near 0 ppm indicating the presence of very few aluminium species in an octahedral environment. These observations, together with those from TEM and XRD, lead to the conclusion that neither significant dealumination nor mesoporosity creation occurred during the calcination of the materials and the reduction of the platinum (Figs. 1a and 1b). Thus, both Pt3/NaEMT and Pt6/NaEMT constituted good supports for the adsorption of molybdenum hexacarbonyl.

3-2. Formation of the Mo Layer Covering the Pt Particles

Supported platinum clusters sinter during ammonia treatment at a temperature as low as 773 K. However, when platinum was covered by molybdenum carbide or nitride, it was apparently protected against sintering during the ammonia treatment. Two molecular probes, dihydrogen chemisorption (18, 19) and benzene hydrogenation, were used to calculate the fraction of Pt atoms exposed and, therefore, the coverage of Pt by Mo carbide or nitride. It

TABLE 1

Physicochemical Characterization of Pure NaEMT and Platinum-Supported NaEMT Zeolite

Samples	Crystallinity (%)	Chemical analysis	NMR Si/Al	Electron microscopy	
				d_p (Å)[a]	EDS[b]
NaEMT	100[c]	$Na_{20}Al_{20}Si_{76}O_{192}$	3.60 (2)	/	Si/Al = 3.7 (1)
Pt3/NaEMT	100[d]	$Pt_1Na_{18}Al_{20}Si_{76}O_{192}$	3.65 (2)	11.7	Pt/Al = 0.06 (1) Si/Al = 3.7 (1)
Pt6/NaEMT	103[d]	$Pt_2Na_{16}Al_{20}Si_{76}O_{192}$	3.63 (4)	11.6	Pt/Al = 0.11 (1) Si/Al = 3.7 (1)

[a] Average particle diameter (d_p) calculated from measurements of more than 1000 particles.
[b] Numbers in brackets represent the standard deviation of seven analyses for each sample.
[c] Crystallinity estimated at 100% and used as reference.
[d] Crystallinity corrected from atomic absorption by the platinum phase.

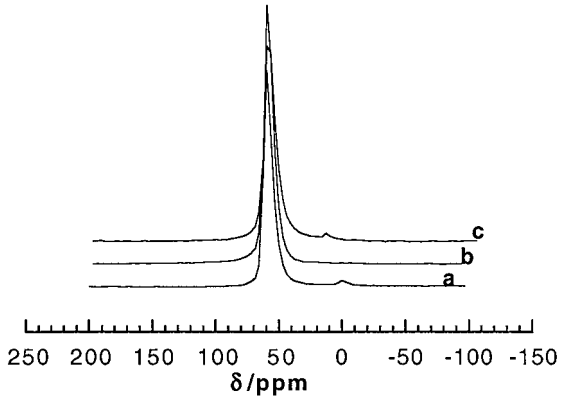

FIG. 1. ^{27}Al NMR spectra of the rehydrated compounds (a) Pt3/NaEMT, (b) Pt6/NaEMT, and (c) PtMoN/NaEMT (Mo/Pt = 3.2).

was checked that, under our experimental conditions, carbide and nitride of molybdenum without platinum neither chemisorbed dihydrogen nor catalyzed benzene. The results of the characterization experiments on the bimetallic samples together with those for Pt3/NaEMT are summarized in Table 2. The turnover rate (v_r) (Table 2, footnote *a*) calculated for benzene hydrogenation over Pt3/NaEMT (100% dispersed) agrees quite well with the rates reported previously for supported Pt catalysts (20, 21). The apparent activation energy deduced from rate measurements between 298 and 340 K was 45.3 ± 1.6 kJ mol^{-1}, which is similar to those values generally encountered in the literature. From the results in Table 2, it can be concluded that Mo loadings of Mo/Pt equal to 1 and 2 are not sufficient to cover the platinum particles. Even though the specific rate for benzene hydrogenation was zero for the decarbonylated sample with Mo/Pt = 3 (FE Pt% = 0), STEM revealed that the molybdenum deposition was inhomogeneous, presumably due to the deposition occurring in one step. Furthermore, the nitrided sample with the same Mo/Pt ratio exhibited some sintered platinum particles on the transmission electron micrographs. The platinum was evidently not sufficiently protected by the molybdenum during nitridation. To avoid migration and sintering of platinum particles outside the zeolite, a three-step preparation method was used. The $Mo(CO)_6$ was successively deposited onto Pt/EMT with each step having an atomic ratio Mo/Pt ≤ 1 and including a thermal decomposition of the molybdenum complex. The final treatment after the last vapor deposition was a nitridation under flowing ammonia at 973 K. It must be emphasized that the atomic ratio Mo/Pt = 3 is between the number of atoms necessary to build the second and the third shell of an icosahedron with a diameter between 7 and 11.1 Å (platinum and molybdenum have the same covalent radius). This method of successive deposition steps was used to prepare other samples for which the platinum loading (Pt6/NaEMT) and the Mo/Pt ratio were higher (Mo/Pt = 3.2, 3.6, and 7.2, see Table 3).

Decarbonylation of $Mo(CO)_6$/NaEMT at 600 K under a partial pressure of H_2 gave a shoulder at about 283.6 eV

TABLE 2

Characterization of Bimetallic Compounds Prepared from 3 wt% Pt on EMT Zeolite

	Treatment	Benzene hydrogenation FE Pt (%)[a]	H_2 chem. H/Pt irrev.	EDS analysis[b]		
				Zeolite area	Particles on zeolite outside	
Pt3/NaEMT	Calcination, reduction	100	1.0 (1)	Pt/Al = 0.06 (1)	—	—
Mo/Pt = 1	Decarbonylation	63	0.8 (1)	Pt/Al = 0.06 (1) Mo/Pt = 1.1 (3)	—	—
Mo/Pt = 2	Decarbonylation	61	0.3 (1)	Pt/Al = 0.04 (1) Mo/Pt = 1.9 (1.0)	Mo	—
Mo/Pt = 3	Decarbonylation	0	0.15 (10)	Pt/Al = 0.05 (1) Mo/Pt = 2.9 (9)	Mo	Mo
Mo/Pt = 3	Nitridation	20	0.15 (10)	Pt/Al = 0.02 (1) Mo/Pt = 2.9 (2.0) Si/Al = 3.7 (1)	Pt ≈ 100 Å	—
Mo/Pt = 3	Mo/Pt = 1 + dec Mo/Pt = 1 + dec Mo/Pt = 1 + nit	5	0.15 (10)	Pt/Al = 0.05 (1) Mo/Pt = 4.1 (1.0) Si/Al = 3.6 (1)	Pt rare	—

[a] Fraction of platinum atoms exposed calculated as 100 times the ratio between the specific rate of the sample (molecules per gram per second) over the turnover rate (equal to 5.4×10^{-2} s^{-1}, as found for Pt3/NaEMT) divided by the total number of Pt atoms per gram of sample.

[b] Average values calculated from 9 or 11 measurements for each sample; the standard deviation is given in parentheses.

TABLE 3

Composition and Crystallinity of Bimetallic Catalysts Prepared from 6 wt% Pt on EMT Zeolite

Samples	Treatments	Chemical analysis	Cryst[a] (%)
Pt6/NaEMT	Calcination, reduction	$Pt_2Na_{16}Al_{20}Si_{76}O_{192}$	103
Pt6/NaEMT Mo/Pt = 3.2	4 × (Mo/Pt = 0.8) decarbonylations	$Pt_{1.8}Mo_{5.6}Na_{16}Al_{20}Si_{76}O_{192}$	91
Pt6/NaEMT Mo/Pt = 3.2	4 × (Mo/Pt = 0.8) decarb. + nitridation	$Pt_{1.8}Mo_{6.4}Na_{16}Al_{20}Si_{76}O_{192}$	93
Pt6/NaEMT Mo/Pt = 3.6	4 × (Mo/Pt = 0.9) decarbonylations	$Pt_2Mo_{7.7}Na_{16}Al_{20}Si_{76}O_{192}$	97
Pt6/NaEMT Mo/Pt = 3.6	4 × (Mo/Pt = 0.9) decarb. + nitridation	$Pt_2Mo_{7.2}Na_{16}Al_{20}Si_{76}O_{192}$	98
Pt6/NaEMT Mo/Pt = 7.2	8 × (Mo/Pt = 0.9) decarbonylations	$Pt_{1.8}Mo_{13.8}Na_{16}Al_{20}Si_{76}O_{192}$	102
Pt6/NaEMT Mo/Pt = 7.2	8 × (Mo/Pt = 0.9) decarb. + nitridation	$Pt_2Mo_{15.4}Na_{16}Al_{20}Si_{76}O_{192}$	103

[a] Cryst, crystallinity (corrected for atomic absorption by the metallic phases).

in the C1*s* XPS peak, indicating the formation of a carbide phase. Earlier work has demonstrated conclusively that treatment of $Mo(CO)_6$/NaEMT with ammonia produced an ultradispersed nitride phase (11). Therefore, these same procedures were used for the final step of preparation of the bimetallic compounds to obtain either a Mo carbide or a Mo nitride layer covering the platinum particles. The XRD patterns of the various samples did not show any damage to the zeolite lattice. Also, no platinum or molybdenum-phase diffraction peak was observed after these treatments. Furthermore, no significant extraframework aluminium was observed by NMR spectroscopy of the PtMoN/EMT sample (Fig. 1c).

Two representative HRTEM micrographs are presented in Fig. 2. The EDS analyses of the samples are given in Table 4 and show that the platinum remains homogeneously distributed (Pt/Al = 0.11, with a low standard deviation) and that the molybdenum has been introduced inside the EMT cages. However, the Mo loading was not as homogeneous as for platinum since the EDS analysis indicated that some spherical nodules found on the external surface of the zeolite were composed mainly of molybdenum. Nevertheless, those nodules were quite rare, even for the highest Mo loading (Mo/Pt = 7.2).

Results from benzene hydrogenation and H_2 chemisorption suggest that the platinum may be covered almost completely at a Mo/Pt ratio as low as 3.2. The average size of Pt–Mo particles clearly showed a shift in the distribution toward a larger diameter after deposition of molybdenum carbide or nitride. This size enhancement is likely due to the addition of molybdenum atoms since the decomposition treatment did not provoke any sintering. Interestingly, once the first layer (nitride or carbide) was formed, deposition of additional molybdenum atoms did not occur. For the higher Mo/Pt ratios (3.6 and 7.2), the average particle size did not increase but remained at about 19 Å in diameter. This particle size, which is greater than the diameter of the zeolite supercage (13.5 Å), probably results from molybdenum atoms adsorbing on Pt clusters at the cage apertures to give a grape-like shape allowed by the particular structure of the EMT zeolite whose cages are directly connected by five apertures to two large supercages and three smaller elliptical supercages. Clearly, there was little affinity for the Mo to be deposited on the covered platinum, and instead Mo was deposited throughout the pores as if there were no platinum. The bimetallic PtMo (carbidized or nitrided) clusters appear to be similar to those that Iwasawa *et al.* call an *eggshell* structure (22) consisting of a platinum core with a Mo carbide or nitride layer. This is in total agreement with the results of Tri *et al.* who have described that addition of Mo on a core of zero valent Pt follows the fcc arrangement (7). Samant *et al.* (23) also confirmed this epitaxial deposition at lower coverage.

Results from X-ray absorption spectroscopy provided additional characterization of the Pt–Mo interaction in the bimetallic samples. Figure 3A shows the Mo K near edge spectra of Mo foil and bulk MoN compared to representative supported Mo and bimetallic (Mo/Pt = 3.2) nitride samples. The broad features of the supported samples are consistent with their high levels of dispersion throughout the zeolite. Derivatives of the near edge spectra, shown in Fig. 3B, reveal information about the average oxidation state of the Mo in the samples. All energies labeled on Fig. 3B are referenced to the first peak in the first derivative of Mo foil. The major peak in the derivative of bulk MoN occurred at 8.4 eV, whereas the major peak in zeolite-supported MoN was observed at 12.8 eV, indicating a higher degree of oxidation for the supported sample. Indeed, the supported nitrides (or carbides) are more properly referred to as oxynitrides (or oxycarbides). The corresponding major

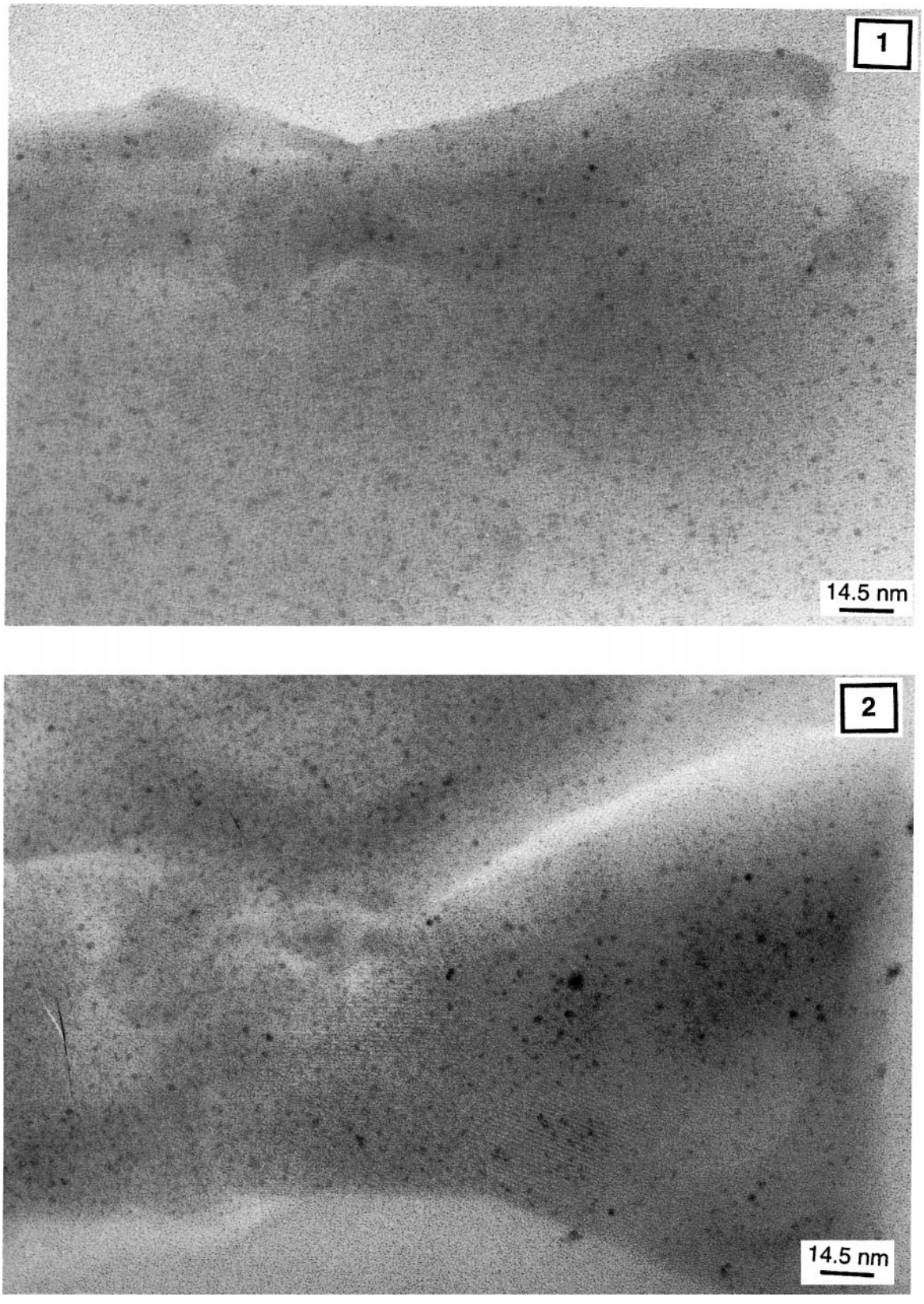

FIG. 2. HRTEM micrographs of ultramicrotome sections of PtMoC/EMT (1) and PtMoN/EMT (2) samples (Mo/Pt = 3.2).

TABLE 4

Effect of Mo Loading and Subsequent Treatments on the Characteristics of Bimetallic Samples

	Treatment	Benzene hydrogenation FE Pt (%)[a]	H_2 chem. H/Pt irrev.[b]	TEM d_p (Å)[c]	EDS analysis	
					Zeolite area[d]	Nodules on zeolite
Pt6/NaEMT	Calcination, reduction	100	1.0	11.6	Pt/Al = 0.10 (2)	—
Mo/Pt = 3.2	Decarbonylation	7	0.01	18.4	Pt/Al = 0.11 (1) Mo/Pt = 2.9 (6) Si/Al = 4.0 (3)	Mo rare
Mo/Pt = 3.2	Decarbonylation + Nitridation	20	0.07	17.0	Pt/Al = 0.12 (2) Mo/Pt = 3.3 (5) Si/Al = 3.8 (4)	—
Mo/Pt = 3.6	Decarbonylation	5	0.06	18.5	Pt/Al = 0.12 (2) Mo/Pt = 2.7 (3) Si/Al = 3.9 (2)	Mo rare $45 < d_p < 100$ (Å)
Mo/Pt = 3.6	Decarbonylation + Nitridation	2.5	0.10	20.2	Pt/Al = 0.11 (1) Mo/Pt = 2.9 (9) Si/Al = 3.7 (2)	Mo rare $45 < d_p < 110$ (Å)
Mo/Pt = 7.2	Decarbonylation	5	0.15	18.6	Pt/Al = 0.11 (1) Mo/Pt = 4.0 (2) Si/Al = 3.7 (2)	Mo $50 < d_p < 150$ (Å)
Mo/Pt = 7.2	Decarbonylation + Nitridation	7	0.15	18.8	Pt/Al = 0.12 (2) Mo/Pt = 6.8 (1.0) Si/Al = 4.3 (2)	Mo $50 < d_p < 125$ (Å)

[a] Fraction of platinum atoms exposed.
[b] Experimental error, ±0.10.
[c] Average particle diameter d_p calculated from measurements of more than 1000 particles.
[d] Average values calculated from 9 or 11 measurements for each sample; standard deviations are in parentheses.

peak in the derivative of the bimetallic sample was found at 10.3 eV, which suggests a greater degree of Mo reduction due to the presence of Pt. The k^3-weighted EXAFS functions and corresponding Fourier transforms of the nitride samples are given in Figs. 4A and 4B. The three major features in the Fourier transform of bulk MoN correspond to the Mo–N distance from 1 to 2 Å, the Mo–Mo distance from 2 to 3 Å, and a higher shell Mo–Mo distance from 3 to 4 Å. The peaks associated with Mo–Mo absorber–backscatterer pairs are greatly diminished in the transform of the supported MoN sample, confirming the very small particle size of the nitride. Interestingly, the peak from 2 to 3 Å was more intense for the sample containing Pt, which may suggest a close interaction between the Mo nitride phase and the underlying Pt cluster. However, this peak may result from both Mo–Mo and Mo–Pt absorber–backscatterer pairs.

Figure 5 presents the Pt LIII near edge spectra of Pt foil, Pt6/NaEMT, and the bimetallic PtMo nitride (Mo/Pt = 3.2) supported on EMT. Even though the maximum in the first derivative of Pt foil was about 0.5 eV lower than that of either supported material, the Pt was evidently well-reduced in both zeolite samples. The broad white line region of the spectrum of supported Pt (Fig. 5b) is due to the creation of unoccupied antibonding states resulting from the adsorption of hydrogen on small metal particles. This phenomenon has been observed previously for zeolite-supported Pt particles and is thoroughly discussed by Samant and Boudart (24). Incorporation of Mo nitride onto the supported Pt clusters modified the Pt near edge spectrum (Fig. 5c) so that it appeared more like Pt foil. This modification in the near edge can be explained by the suppression of dihydrogen chemisorption on the Pt due to the presence of Mo or the sintering of Pt particles to give large metal aggregates. However, results from electron microscopy suggest that Mo deposition and nitridation did not sinter the Pt clusters. The EXAFS region of the spectrum can be used to resolve this issue. The k^3-weighted EXAFS functions and corresponding Fourier transforms of the supported Pt samples are shown in Figs. 6A and 6B. Curve fitting of the first shell Pt–Pt contribution to the EXAFS function of Pt6/EMT gave a coordination number of 5.5, a Pt–Pt interatomic distance of 2.75 Å, and a change in Debye–Waller factor ($\Delta\sigma^2$) of 0.0023 $Å^2$ relative to Pt foil. The low coordination number and positive change in Debye–Waller factor are consistent with earlier structural studies that concluded small Pt particles were formed on the zeolite (8). The highly modified EXAFS function in Fig. 6A(b) and Fourier transform in Fig. 6B(b) indicate the presence of another heavy scatterer

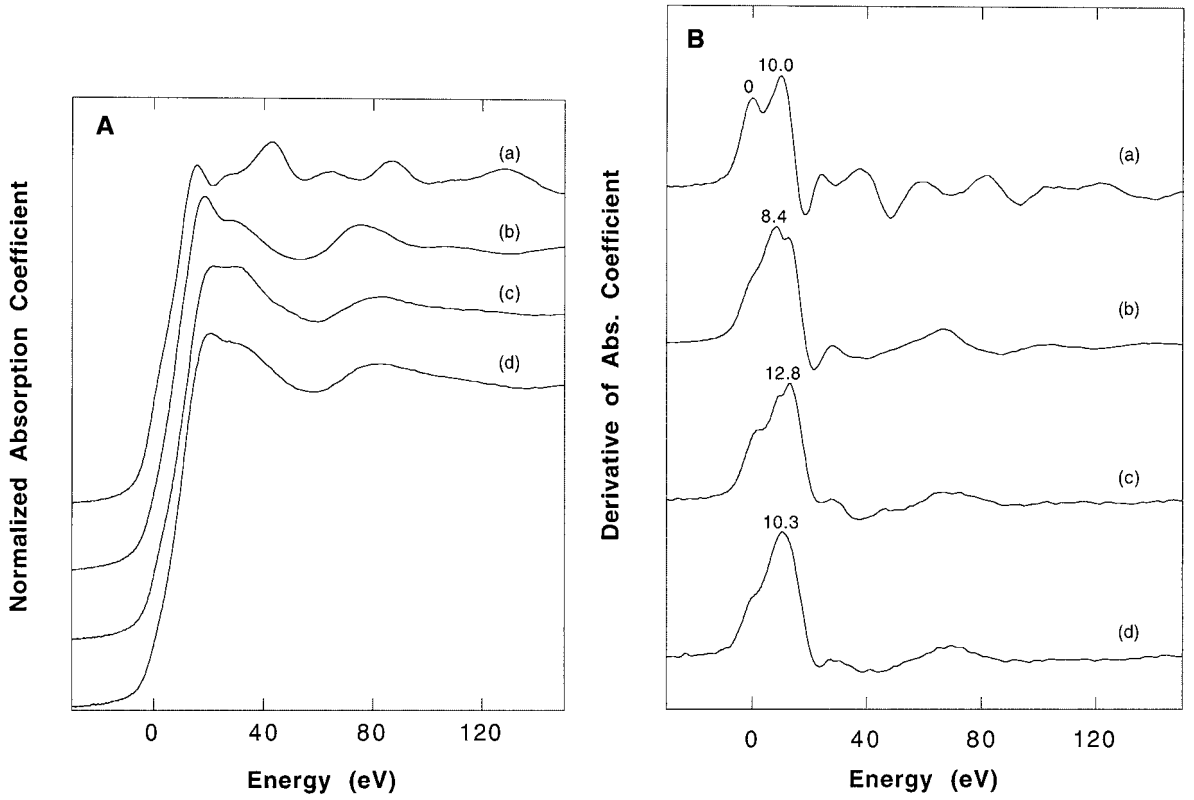

FIG. 3. (A) Molybdenum K edge spectra of (a) Mo foil, (b) bulk δ-MoN, (c) MoN/NaEMT, and (d) PtMoN/EMT (Mo/Pt = 3.2). Zero in energy is defined relative to the first maximum in the derivative of the edge spectrum of Mo foil. (B) First derivatives of Mo K edges of (a) Mo foil, (b) bulk δ-MoN, (c) MoN/NaEMT, and (d) PtMoN/EMT (Mo/Pt = 3.2). Zero in energy is defined relative to the first maximum in the derivative of the edge spectrum of Mo foil.

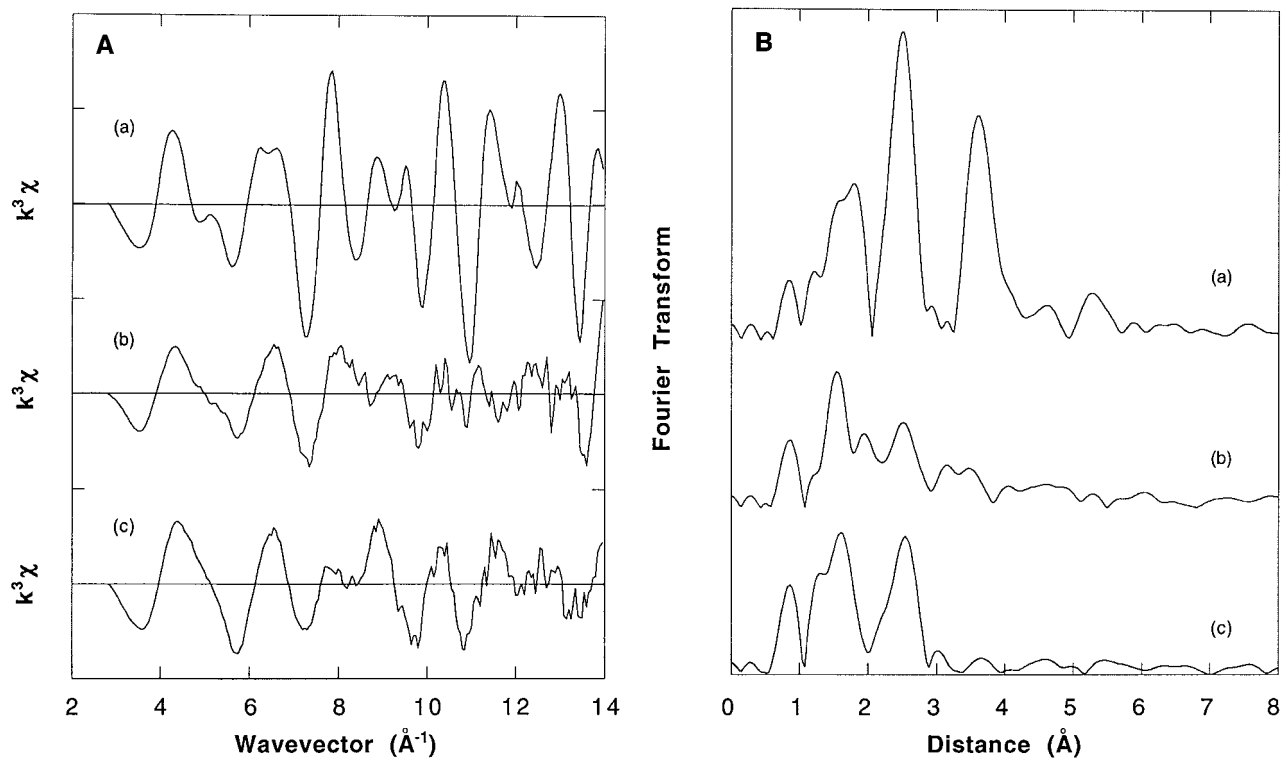

FIG. 4. (A) Molybdenum K EXAFS functions, $k^3\chi(k)$, for (a) bulk δ-MoN, (b) MoN/NaEMT, and (c) PtMoN/EMT (Mo/Pt = 3.2). (B) Fourier transforms of Mo K EXAFS functions, not corrected for phase shifts, for (a) bulk δ-MoN, (b) MoN/NaEMT, and (c) PtMoN/EMT (Mo/Pt = 3.2).

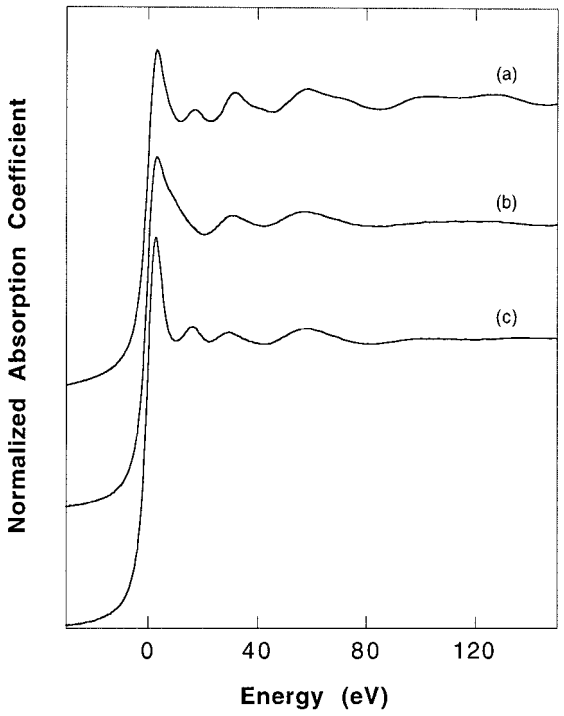

FIG. 5. Platinum LIII edge spectra of (a) Pt foil, (b) Pt6/NaEMT, and (c) PtMoN/EMT (Mo/Pt = 3.2). Zero in energy is defined relative to the maximum in the derivative of the edge spectrum of Pt foil.

in the average first coordination shell of Pt. These results for the bimetallic sample clearly show that the decrease in dihydrogen chemisorption, the decrease in benzene hydrogenation activity, and the modification of Pt LIII edge structure are due to the presence of Mo on Pt instead of excessive sintering.

3-3. Catalytic Reaction of n-Heptane

(a) Monometallic Pt/NaEMT catalysts. As shown in Table 5, the site time yield for *n*-heptane isomerization over Pt/NaEMT was independent of the platinum loading, thus confirming the absence of internal diffusion effects on the kinetic data.

The supported platinum catalysts, Pt3/NaEMT and Pt6/NaEMT, were prepared by cationic exchange into a nonacidic EMT zeolite; however, subsequent reduction of the platinum ions by dihydrogen necessarily induces the formation of a number of protonic acid sites in the zeolite that scales with the loading of platinum (10, 25). Despite the existence of these acidic sites on Pt3/NaEMT and Pt6/NaEMT, the product distributions reported in Table 5 indicate that *n*-heptane was converted mainly according to a monofunctional mechanism on metallic sites. If the activity and product distribution for a bifunctional Pt3/NaHEMT sample (75% H^+ exchange, Table 5) are compared to those for the standard Pt/NaEMT catalysts, one finds a higher conversion on the acidic material at constant contact time and a higher fraction of midscission products (C3 + C4) resulting from cracking reactions on acid sites. Moreover, the isoC4/*n*C4 ratio, which correlates with an acidic isomerization route (26), is negligible ($i/n = 0.2$) for Pt3/NaEMT and Pt6/NaEMT, whereas the relatively high isoC4/*n*C4 ratio ($i/n = 5.4$) for Pt3/NaHEMT, is typical of the bifunctional mechanism involving both metallic and acidic sites.

It is also well-known that the extent of bifunctional catalysis depends on the ratio of acidic sites to metallic sites (27). In our case, the two protons generated during reduction of each exchanged Pt ion are clearly insufficient to significantly depress the aromatization reaction, whose mechanism is monofunctional on metallic sites (28, 29). We conclude, therefore, that *n*-heptane scission over Pt*x*/NaEMT catalysts does not follow a bifunctional mechanism but instead occurs mainly on the metallic sites. The very few acidic sites have only a weak effect on the catalytic activity when the support is initially in the sodium form (NaEMT). These materials will be considered in this work as reference monofunctional Pt catalysts.

TABLE 5

Product Distribution during *n*-Heptane Reaction on Pt_x/EMT Catalysts (623 K, H_2/*n*C7 = 17, Contact Time = 1.3×10^{-3} min)

		Isomerization iso-Heptanes (%)					Dehyd	Arom	Hydrogenolysis–cracking Light products (%)		
Samples	Conv (%)	2 & 3m	2,3	2,4	2,2	Et	C7=	Toluene	C1 + C6	C2 + C5	C3 + C4[a]
Pt3/NaEMT	18.1			80.8			1.2	13.1		4.9	($i/n = 0.3$)
		93.8	0.2	3.4	2.3	—			9.4	29.4	61.2
Pt6/NaEMT	18.4			77.1			1.6	14.3		7.0	($i/n = 0.2$)
		96.3	0.1	3.3	2.6	—			28.6	26.2	45.1
Pt3/NaHEMT	46.4			83.1			0.3	4.3		12.3	($i/n = 5.4$)
		88.0	0.4	8.6	0.3	2.6			2.3	2.3	95.4

Note. Conv, total conversion; Dehyd, dehydrogenation; Arom, aromatization. 2 & 3m, 2- and 3-methylhexanes; 2,3, 2,3-dimethyl pentane; 2,4, 2,4-dimethyl pentane; 2,2, 2,2-dimethyl pentane; Et, ethylpentane; C7=, heptenes; C*x*, hydrocarbon skeleton with *x* atoms of carbon.

[a] Number in parentheses is the i/n value representing the isobutane on *n*-butane molar ratio.

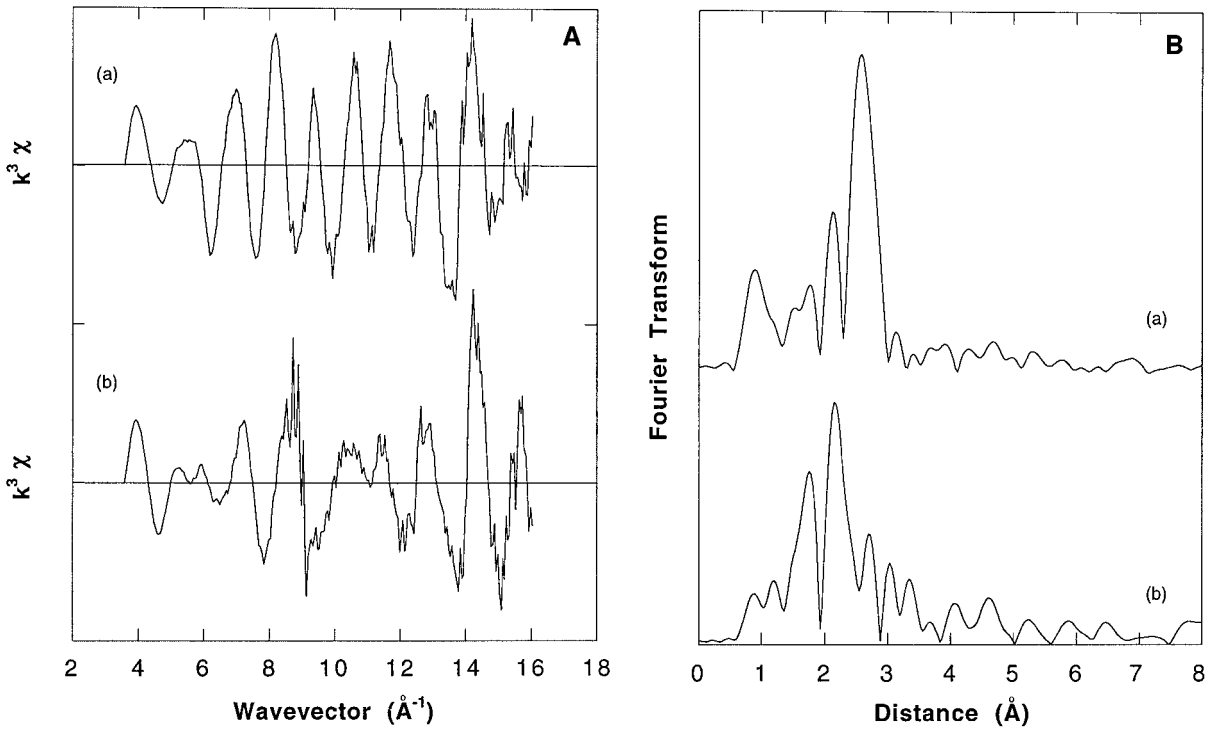

FIG. 6. (A) Platinum LIII EXAFS functions, $k^3\chi(k)$, for (a) Pt6/NaEMT and (b) PtMoN/EMT (Mo/Pt = 3.2). (B) Fourier transforms of Pt LIII EXAFS functions, not corrected for phase shifts, for (a) Pt6/NaEMT and (b) PtMoN/EMT (Mo/Pt = 3.2).

(b) Bimetallic PtMo(N or C)/NaEMT catalysts. The conversion in *n*-heptane (623 K) over monometallic and bimetallic catalysts is shown as a function of time on stream in Fig. 7. The presence of some acidic sites generated by the reduction of the Pt precursor may have enhanced the formation of coke leading to deactivation of the catalysts. Nevertheless, the catalyst activity decreased in all cases when Pt was covered by Mo carbide or nitride, with the nitride catalysts being the least active.

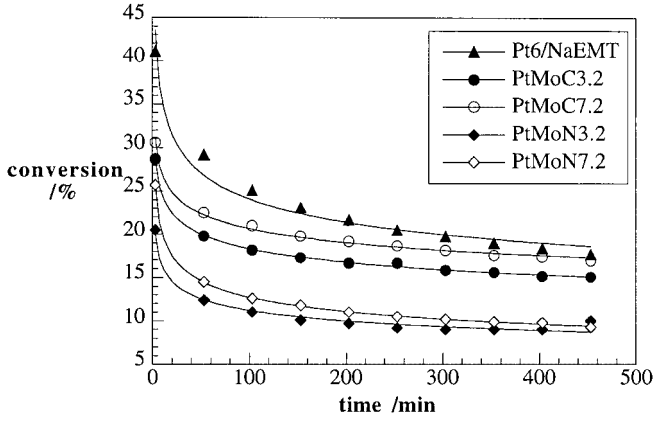

FIG. 7. Evolution of the activity as a function of time-on-stream for the bimetallic supported compounds in *n*-heptane conversion (623 K).

Normalization of reaction rates measured over the bimetallic catalysts is problematic due to the ambiguities associated with dihydrogen chemisorption on Pt in contact with partially reduced Mo. Therefore, we have based reaction rates for the bimetallic catalysts on the number of surface active sites counted by the benzene hydrogenation reaction, as reported in Table 4. For supported Mo nitride (30) and carbide, the reaction rate was based on the total number of Mo atoms in the sample. The site time yields for *n*-heptane reactions on the various bulk and supported catalysts are summarized in Tables 6A and 6B. The observed rates over bulk and supported Mo carbide and nitride are orders of magnitude lower than that of supported

TABLE 6A

Site-Time Yields (STY) for *n*-Heptane Reactions at 623 K after 6 h on Stream under Standard Experimental Conditions

	Samples				
	Mo_2N bulk	Mo_2C bulk	MoN/ NaEMT	MoC/ NaEMT	Pt/ NaEMT
STY (10^{-4} s^{-1})	1.6[a]	2.5[a]	1.7[b]	1.5[b]	500[c]

[a] Calculated assuming 10^{+15} sites cm^{-2}.
[b] Calculated assuming 100% fraction of Mo atoms exposed.
[c] Calculated assuming 100% fraction of Pt atoms exposed.

TABLE 6B

Site-Time Yields for *n*-Heptane Reactions at 623 K after 6 h on Stream under Standard Experimental Conditions[a]

	Samples				
	$Pt(MoN)_{3.2}$/NaEMT	$Pt(MoC)_{3.2}$/NaEMT	$Pt(MoN)_{7.2}$/NaEMT	$Pt(MoC)_{7.2}$/NaEMT	Pt/NaEMT
STY (s^{-1})	0.10	0.52	0.33	0.82	0.05

[a] Calculated for the fraction of platinum atom exposed in benzene hydrogenation (Table 4).

Pt. However, the formation of a bimetallic carbide or nitride appears to increase the specific rate on the small area of exposed Pt and/or to increase the activity of the carbide or nitride phase. The specific rate increased with loading of Mo carbide or nitride (Table 6B), which suggests the important role of the Mo phase in the reaction of *n*-heptane.

Earlier studies on supported bimetallic catalysts (Pt + Mo or W) have shown that each component can present a new catalytic function. Generally, hydrogenation and hydrogenolysis reactions are enhanced, whereas dehydrogenation reactions are depressed. In those works, the best efficiency was obtained for a Pt/(Pt + Mo) ratio equal to 0.5 (19, 31–35) or for an alloy formation (36). High loadings of an inactive metal on an active metal are generally harmful to catalysis, as demonstrated by the lack of activity of molybdenum layers on a platinum core in the hydrogenation of ethylene and the hydrogenolysis of ethane (22).

The product distributions for *n*-heptane reactions on the bimetallic catalysts at 623 K are presented in Table 7. The results are reported after 3 min on stream, when the catalysts were not drastically poisoned by coke, and after 6 h, when a quasisteady state was reached. These results can be compared with those of Pt6/NaEMT (Table 5) and supported Mo nitride or carbide (Table 7). In contrast to the reaction on Pt6/NaEMT, very little aromatization was observed on the bimetallic catalysts. The presence of a molybdenum carbide or nitride layer strongly inhibits the dehydrocyclization reaction. According to Leclercq *et al.* (35) and Woo *et al.* (37), this decrease in aromatization confirms that the platinum clusters are covered by a molybdenum phase. Furthermore, the fraction of hydrogenolysis

TABLE 7

Product Distribution during *n*-Heptane Reaction on the Bimetallic Catalysts (623 K, $H_2/nC7 = 17$, Contact Time $= 1.2 \times 10^{-3}$ min)

Samples	Conv (%)	Isomerization iso-Heptanes (%)					Dehyd C7=	Arom Toluene	Hydrogenolysis–cracking Light products (%)		
		2 & 3m	2,3	2,4	2,2	Et			C1 + C6	C2 + C5	C3 + C4[a]
MoN/NaEMT	1.3			55.6			22.1	—		22.3	($i/n = 0$)
		86.1	—	—	—	13.9			20.0	24.4	55.6
PtMoN3.2(4 × 0.8)/NaEMT	20.5			29.2			1.1	3.4		66.0	($i/n = 0.03$)
		93.1	—	2.7	3.6	—			34.5	32.1	33.4
	9.0			49.5			2.3	5.0		43.2	($i/n = 0$)
		93.1	—	2.7	3.6	—			47.4	28.1	24.5
PtMoN7.2(8 × 0.9)/NaEMT	25.7			24.8			—	6.1		69.1	($i/n = 0.03$)
		86.4	0.5	2.0	4.2	6.0			35.4	32.3	32.3
	9.9			45.9			1.3	4.5		48.2	($i/n = 0$)
		96.3	—	1.4	2.2	—			47.0	28.9	24.1
MoC/NaEMT	1.0			77.6			18.6	—		3.8	($i/n = 0$)
		85.1	—	—	—	14.9			100	—	—
PtMoC3.2(4 × 0.8)/NaEMT	28.7			46.2			0.5	5.9		47.4	($i/n = 0.06$)
		94.6	—	3.4	1.7	—			39.9	29.6	30.5
	15.6			74.9			1.3	2.9		20.9	($i/n = 0.10$)
		96.5	—	2.9	0.6	—			51.8	25.4	22.8
PtMoC7.2(8 × 0.9)/NaEMT	30.6			54.8			0.6	5.7		38.9	($i/n = 0.10$)
		93.2	—	4.6	2.9	1.3			38.7	30.0	31.2
	17.6			77.5			1.1	2.7		18.7	($i/n = 0.20$)
		94.7	—	3.7	1.0	1.0			50.0	26.0	24.0

Note. Conv, total conversion; Dehyd, dehydrogenation; Arom, aromatization. 2 & 3m, 2- and 3-methylhexanes; 2,3, 2,3-dimethyl pentane; 2,4, 2,4-dimethyl pentane; 2,2, 2,2-dimethyl pentane; Et, ethylpentane; C7=, heptenes; C*x*, hydrocarbon skeleton with *x* atoms of carbon.

[a] Number in parentheses is the i/n value representing the isobutane to *n*-butane molar ratio.

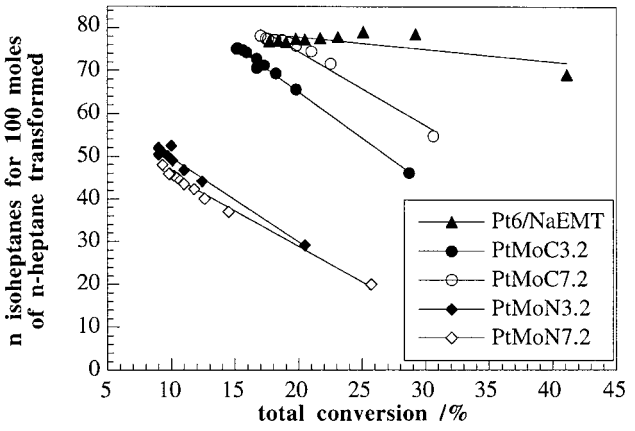

FIG. 8. Evolution of the *n*-heptane isomerization selectivity with total conversion for the bimetallic supported compounds.

products increased over the bimetallic catalysts, particularly when molybdenum had been nitrided. This phenomenon can not be attributed to electron-deficient platinum because Tri *et al.* (7) have shown that any electrophilic character of the platinum disappeared once Mo atoms were added. Indeed, our Pt LIII edge spectra in Fig. 5 support the idea that Mo-covered Pt clusters are metallic. Earlier work has suggested that the Mo atoms act as strong adsorption sites for hydrocarbons, thus explaining the enhanced hydrogenolysis activity of PtMo/Y catalysts in *n*-butane conversion (32). However, total conversion of *n*-heptane over PtMoC/NaEMT and PtMoN/NaEMT was lower than that over Pt6/NaEMT (Fig. 7) because very few Pt atoms were accessible for the dissociation of dihydrogen molecules into adsorbed hydrogen atoms, which must subsequently react with species adsorbed on the Mo sites. Interestingly, a major difference in the hydrogenolysis function of the bimetallic samples compared to supported Pt is the distribution of light products (Tables 5 and 7). Addition of MoC or MoN to Pt appears to shift the distribution toward products resulting from terminal bond scission.

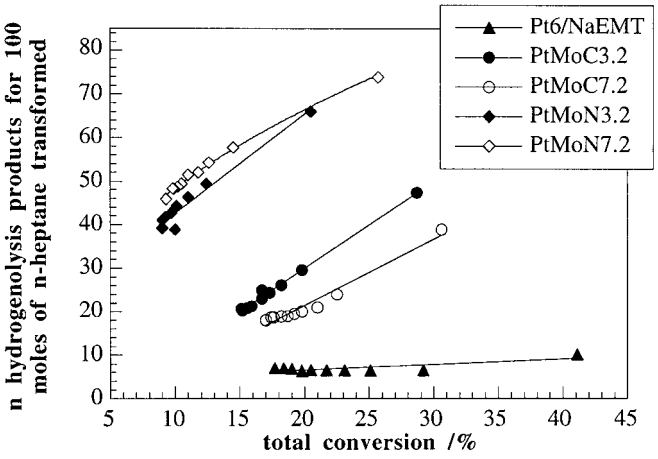

FIG. 9. Evolution of the *n*-heptane hydrogenolysis selectivity with total conversion for the bimetallic supported compounds.

Another reaction of *n*-heptane on the bimetallic catalysts is isomerization. Whereas selectivity to iso-heptanes remained constant with the level of conversion (or time on stream) over Pt6/NaEMT, the selectivity over the bimetallic catalysts decreased with increasing conversion (Fig. 8). Figure 9 reveals the opposite trend in the fraction of hydrogenolysis products formed over the bimetallic catalysts. Since the number of iso-heptane molecules produced per *n*-heptane feed was fairly constant with time, the isomerization reaction was not affected by deactivation. In contrast, the number of light molecules decreased with time and accounted for most of the decrease in reaction conversion with time on stream.

4. CONCLUSIONS

Bimetallic Pt/Mo carbide and nitride clusters supported on EMT zeolite have been synthesized and thoroughly characterized in this work. In particular, the bimetallic clusters were composed of nanometer-sized Pt cores covered by Mo carbide or nitride layers. High coverage of the predispersed platinum particles required successive $Mo(CO)_6$ vapor deposition steps, each with an atomic Mo/Pt ratio not exceeding unity. The molybdenum hexacarbonyl complex had to be decarbonylated between each deposition and the last step was followed either by decomposition of $Mo(CO)_6$ under dihydrogen to form a carbide or by reaction with ammonia to form a nitride. Results from H_2 chemisorption and benzene hydrogenation confirmed that nearly complete coverage of Pt clusters can be accomplished with a Mo/Pt ratio equal to 3.2. Addition of Mo above this ratio resulted in formation of Mo clusters dispersed throughout the zeolite.

The coverage of the Pt clusters by a Mo carbide or nitride layer was also indicated by the unique performance of the bimetallic samples in the catalytic reactions of *n*-heptane. For example, aromatization was suppressed on the bimetallic samples compared to supported Pt. In addition, the bimetallic catalysts were quite active for *n*-heptane isomerization to 2-methyl and 3-methyl hexanes, even after 8 h on stream. The hydrogenolysis of *n*-heptane on the bimetallic clusters (nitrided or carbidized) was characteristic of an efficient metallic function since the midscission C3 and C4 products were not favored.

The surprising specific activity encountered for PtMoC/NaEMT and PtMoN/NaEMT revealed a beneficial influence of the Pt core. The low thickness of the carbide or nitride phase (about 0.3 nm) in PtMoC/NaEMT and PtMoN/NaEMT allowed for a synergistic influence of the Mo phase on the small areas of exposed Pt and/or a direct activation of the nitride or carbide for catalysis.

ACKNOWLEDGMENTS

The authors greatly acknowledge Professor M. Boudart for fruitful discussions during this work. They wish to address their thanks to Mrs. J. Maquet for her assistance in acquiring NMR data and to Dr. George Meitzner (Edge Analytical, Inc., Stanford, CA) for his aid in the collection of X-ray absorption spectra. The help of Mrs. P. Beaunier and Mr. M. Lavergne for STEM-EDS and TEM measurements is also greatly appreciated. R.J.D. acknowledges the U.S. National Science Foundation (CTS-9729812) for partial support of this work.

REFERENCES

1. Oyama, S. T., and Haller, G., *in* "Catalysis, A Specialist Periodical Report, 1981," Vol. 5, p. 333. The Chemical Society, London, 1982.
2. Leclercq, L., *in* "Surface Properties and Catalysis by Non-Metals" (J. P. Bonnelle *et al.*, Eds.), p. 433. Reidel, Dordrecht, 1983.
3. Volpe, L., Oyama, S. T., and Boudart, M., *in* "Preparation of Catalysts III" (G. Poncelet, P. Grange, and P. A. Jacobs, Eds.), p. 147. Elsevier, Amsterdam, 1983.
4. Volpe, L., and Boudart, M., *J. Solid State Chem.* **59**, 332 (1985).
5. Jaggers, C. H., Michaels, J. N., and Stacy, A. M., *Chem. Mater.* **2**, 150 (1990).
6. Ledoux, M. J., Pham-Huu, C., Delporte, P., Blekkan, E. A., York, A. P. E., Derouane, E. G., and Fonseca, A., *in* "Studies in Surface Science and Catalysis. Science and Technology in Catalysis 1994" (Y. Izumi, H. Arai, and M. Iwamoto, Eds.), Vol. 92, p. 81. Elsevier, Amsterdam, 1995.
7. Tri, T. M., Candy, J.-P., Gallezot, P., Massardier, J., Primet, M., Védrine, J. C., and Imelik, B., *J. Catal.* **79**, 396 (1983).
8. Ihee, H., Bécue, T., Ryoo, R., Potvin, C., Manoli, J.-M., and Djéga-Mariadassou, G., *Stud. Surf. Sci. Catal.* **84**, 765 (1994).
9. Delprato, F., Delmotte, L., Guth, J. L., and Huve, L., *Zeolites* **10**, 546 (1990).
10. Dalla Betta, R. A., and Boudart, M., *in* "Proceedings, 5th International Congress on Catalysis, Miami Beach, 1972" (J. W. Hightower, Ed.), Vol. 2, p. 1329. North Holland, Amsterdam, 1973.
11. Bécue, T., Manoli, J.-M., Potvin, C., Djéga-Mariadassou, G., and Delamar, M., *J. Phys. Chem. B* **101**, 6429 (1997).
12. Chatelain, T., Patarin, J., Soulard, M., Guth, J.-L., and Schultz, P., *Zeolites* **15**, 90 (1995).
13. Léglise, J., Manoli, J.-M., Potvin, C., Djéga-Mariadassou, G., and Cornet, D., *J. Catal.* **141**, 275 (1995).
14. Yates, D. J. C., and Sinfelt, J. H., *J. Catal.* **8**, 348 (1967).
15. Benson, J. E., and Boudart, M., *J. Catal.* **4**, 704 (1965).
16. Boudart, M., Aldag, A., Benson, J. E., Dougharty, N. A., and Girvin Harkins, C., *J. Catal.* **6**, 92 (1966).
17. Boudart, M., *in* "Advances in Catalysis" (D. D. Eley, H. Pines, and P. B. Weisz, Eds.), Vol. 20, p. 153. Academic Press, New York, 1969.
18. Tri, T. M., Thesis, University Lyon I, France, 1982.
19. Leclercq, G., Romero, T., Pietrzyk, S., Grimblot, J., and Leclercq, L., *J. Mol. Catal.* **25**, 67 (1984).
20. Dorling, T. A., and Moss, R. L., *J. Catal.* **6**, 111 (1966).
21. Gallezot, P., Datka, J., Massardier, J., Primet, M., and Imelik, B., *in* "Proceedings, 6th International Congress on Catalysis, London, 1976" (G. C. Bond, P. B. Wells, and F. C. Tompkins, Eds.), Vol. 2, p. 696. The Chemical Society, London, 1977.
22. Liu, T., Asakura, K., Lee, U., Matsui, Y., and Iwasawa, Y., *J. Catal.* **135**, 367 (1992).
23. Samant, M. G., Bergeret, G., Meitzner, G., Gallezot, P., and Boudart, M., *J. Phys. Chem.* **92**, 3547 (1988).
24. Samant, M. G., and Boudart, M., *J. Phys. Chem.* **95**, 4070 (1991).
25. Tzou, M. S., Teo, B. K., and Sachtler, W. M. H., *J. Catal.* **113**, 220 (1988).
26. Lemos, F., Ramoa Ribeiro, F., Kern, M., Giannetto, G., and Guisnet, M., *Appl. Catal.* **29**, 43 (1987).
27. Guisnet, M., Alvarez, F., and Giannetto Pace, G., *Catal. Today* **1**, 415 (1987).
28. Mielczarski, E., Hong, S. B., Davis, R. J., and Davis, M. E., *J. Catal.* **134**, 359 (1992).
29. Davis, R. J., *Heterog. Chem. Rev.* **1**, 41 (1994).
30. Becue, T., Manoli, J. M., Potvin, C., and Djega-Mariadassou, *J. Catal.* **170**, 123 (1997).
31. Tri, T. M., Massardier, J., Gallezot, P., and Imelik, B., *J. Catal.* **85**, 244 (1984).
32. Tri, T. M., Massardier, J., Gallezot, P., and Imelik, B., *J. Mol. Catal.* **25**, 151 (1984).
33. Guo, X., Yang, Y., Den, M., Li, H., and Lin, Z., *J. Catal.* **99**, 218 (1986).
34. Leclercq, G., El Gharbi, A., and Pietrzyk, S., *J. Catal.* **144**, 118 (1993).
35. Leclercq, G., El Gharbi, A., Gengembre, L., Romero, T., Leclercq, L., and Pietrzyk, S., *J. Catal.* **148**, 550 (1994).
36. Yermakov, Y. I., Kusnetsov, B. N., and Ryndin, Y. A., *J. Catal.* **42**, 73 (1976).
37. Yang, O. B., Woo, S. I., and Hwang, I. C., *Catal. Lett.* **19**, 39 (1993).